DMD Fast Forward. Published on May 19, 2023 as DOI: 10.1124/dmd.122.000980
This article has not been copyedited and formatted. The final version may differ from this version.

Biodistribution of Lipid 5, mRNA, and Its Translated Protein Following Intravenous Administration of mRNA-Encapsulated Lipid Nanoparticles in Rats

Lei Ci, Marjie Hard, Hannah Zhang, Srujan Gandham, Serenus Hua, John Wickwire, Tod Wehrman, Richard Slauter, Andrew Auerbach, Matthew Kenney, Greg Mercer, Tracy Hendrick, Örn Almarsson, Eugene Cheung, Douglas Burdette*

Moderna, Inc., Cambridge, Massachusetts, USA (LC, HZ, SG, SH, JW, AA, MK, GM, EC, and DB)

Praxis Precision Medicines, Boston, Massachusetts, USA (MH)

Charles River Laboratories, Mattawan, Michigan, USA (TW and RS)

Duke University, Durham, North Carolina, USA (TH)

Lyndra Therapeutics, Cambridge, Massachusetts, USA (OA)

Primary laboratory of origin: Moderna, Inc.

Downloaded from dmd.aspetjournals.org at ASPET Journals on April 20, 2024

DMD Fast Forward. Published on May 19, 2023 as DOI: 10.1124/dmd.122.000980
This article has not been copyedited and formatted. The final version may differ from this version.

Running title: Biodistribution of Lipid in Rats

Corresponding author:

Douglas Burdette

Moderna, Inc.

200 Technology Square

Cambridge, MA, 02139

USA

Telephone: 617-218-7613

E-mail: Doug.Burdette@modernatx.com

Target journal: *Drug Metabolism and Disposition*

Number of text pages: 17

Number of tables: 3

Number of supplementary tables: 4

Number of figures: 6

Number of supplementary figures:10

Number of references: 36

Number of words in the Abstract: 245

Number of words in the Significance statement: 76

Downloaded from dmd.aspetjournals.org at ASPET Journals on April 20, 2024

DMD Fast Forward. Published on May 19, 2023 as DOI: 10.1124/dmd.122.000980
This article has not been copyedited and formatted. The final version may differ from this version.

Number of words in the Introduction: 853

Number of words in the Discussion: 1492

Nonstandard abbreviations

BMF, bone marrow femur

BQL, below limit of quantitation

C_{max}, maximum concentration

IV, intravenous

LE, Long-Evans

LNP, lipid nanoparticle

Lipid 5, heptadecan-9-yl 8-((2-hydroxyethyl)(8-(nonyloxy)-8-oxooctyl)amino)octanoate

MS, mass spectrometry

MS/MS, tandem mass spectrometry

PEG, polyethylene glycol

QWBA, quantitative whole-body autoradiography

SD, Sprague Dawley

Downloaded from dmd.aspetjournals.org at ASPET Journals on April 20, 2024

DMD Fast Forward. Published on May 19, 2023 as DOI: 10.1124/dmd.122.000980
This article has not been copyedited and formatted. The final version may differ from this version.

ABSTRACT

RNA-based therapeutics and vaccines represent a novel and expanding class of medicines, the success of which depends on the encapsulation and protection of mRNA molecules in lipid nanoparticle (LNP)–based carriers. With the development of mRNA-LNP modalities, which can incorporate xenobiotic constituents, extensive biodistribution analyses are necessary to better understand the factors that influence their *in vivo* exposure profiles. This study investigated the biodistribution of heptadecan-9-yl 8-((2-hydroxyethyl)(8-(nonyloxy)-8-oxooctyl)amino)octanoate (Lipid 5)—a xenobiotic amino lipid— and its metabolites in male and female pigmented (Long-Evans) and nonpigmented (Sprague Dawley) rats by using quantitative whole-body autoradiography (QWBA) and liquid chromatography–tandem mass spectrometry (LC-MS/MS) techniques. After intravenous injection of Lipid 5-containing LNPs, ^{14}C-containing Lipid 5 ([^{14}C]Lipid 5) and radiolabeled metabolites ([^{14}C]metabolites) were rapidly distributed, with peak concentrations reached within 1 hour in most tissues. After 10 hours, [^{14}C]Lipid 5 and [^{14}C]metabolites concentrated primarily in the urinary and digestive tracts. By 24 hours, [^{14}C]Lipid 5 and [^{14}C]metabolites were localized almost exclusively in the liver and intestines, with few or no concentrations detected in non-excretory systems, which is suggestive of hepatobiliary and renal clearance. [^{14}C]Lipid 5 and [^{14}C]metabolites were completely cleared within 168 hours (7 days). Biodistribution profiles were similar between QWBA and LC-MS/MS techniques, pigmented and nonpigmented rats, and male and female rats, excluding the reproductive organs. In conclusion, the rapid clearance through known excretory systems, with no evidence of redistribution for Lipid 5 or accumulation of [^{14}C]metabolites, provides confidence for the safe and effective use of Lipid 5-containing LNPs.

Downloaded from dmd.aspetjournals.org at ASPET Journals on April 20, 2024

DMD Fast Forward. Published on May 19, 2023 as DOI: 10.1124/dmd.122.000980
This article has not been copyedited and formatted. The final version may differ from this version.

SIGNIFCANCE STATMENT

This study demonstrates the rapid, systemic distribution of intact and radiolabeled metabolites of Lipid 5, a xenobiotic amino lipid component of novel mRNA-LNP medicines, and its effective clearance without substantial redistribution after intravenous administration; additionally, findings were consistent between different mRNAs encapsulated within LNPs of similar composition. This study confirms the applicability of current analytical methods for lipid biodistribution analyses, and taken together with appropriate safety studies, supports the continued use of Lipid 5 in mRNA-medicines.

Downloaded from dmd.aspetjournals.org at ASPET Journals on April 20, 2024

DMD Fast Forward. Published on May 19, 2023 as DOI: 10.1124/dmd.122.000980
This article has not been copyedited and formatted. The final version may differ from this version.

INTRODUCTION

RNA-based therapeutics and vaccines represent a novel and expanding class of medicines that have been invaluable during the coronavirus disease 2019 (COVID-19) pandemic. The global deployment of mRNA COVID-19 vaccines was a prominent milestone for those modalities, building confidence in mRNA research and further substantiating investigations of other mRNA-based medicines, such as enzyme replacement and enhanced cell therapies (Damase et al., 2021). The success of these mRNA therapies depends on their encapsulation in lipid nanoparticles (LNPs), assisting in the transport of exogenous nucleic acids to tissues while simultaneously preventing degradation by endo- and exonucleases (Guevara et al., 2020; Hou et al., 2021). Lipid nanoparticles are non-covalent assemblies of multiple molecular components and are typically composed of ionizable lipids, phospholipids, cholesterol, and polyethylene glycol (PEG)-functionalized lipids (Lee et al., 2013; Hassett et al., 2019; Hou et al., 2021).It has been established that xenobiotic components, such as PEG-functionalized and ionizable lipids stabilize LNP formulation throughout manufacturing and storage, assist in cell surface binding, cellular uptake, and facilitate mRNA endosomal escape (Chan et al., 2012; Shi et al., 2021; Kalyanram et al., 2022). However, studies that assess the *in vivo* fates of LNP-mRNA formulations have focused on the mRNA distribution, and only to a much lesser extent, the biodistribution and clearance of LNP components and their metabolites (Hou et al., 2021). A comprehensive analysis to evaluate the biodistribution and clearance of both the mRNA and LNP constituents is crucial to fully assess the safety and efficacy of these components in both pre-clinical and clinical settings and inform the continued development of improved mRNA-LNP based medicines.

Downloaded from dmd.aspetjournals.org at ASPET Journals on April 20, 2024

DMD Fast Forward. Published on May 19, 2023 as DOI: 10.1124/dmd.122.000980
This article has not been copyedited and formatted. The final version may differ from this version.

As studies into LNP formulations continue, emerging evidence suggests that LNPs have the potential for organ- and tissue-specific tropism of mRNA-based medicines (Rostami et al., 2014; Veiga et al., 2020; Tombacz et al., 2021). The tissue-specific distribution could potentially be facilitated by multiple factors, including LNP particle size, lipid components, and incorporation of specific targeting proteins, such as monoclonal antibodies on the LNP surface (Veiga et al., 2020; Zhang et al., 2021; Di et al., 2022). Although these properties of LNPs are enticing for future drug development, reports have identified variability in delivery of these constructs with greater inflammatory responses associated with the use of xenobiotic lipids which is not apparent with naturally-occurring LNP components (Ndeupen et al., 2021). As naturally occurring LNP components (e.g., lipids, cholesterol, cholesterol esters) undergo *in vivo* processing similar to that of endogenous analogs and xenobiotic lipid clearance routes are typically unknown (Scioli Montoto et al., 2020), a thorough assessment of safety and reactogenicity after LNP administration is needed. It is thus crucial that studies focus on both the primary biodistribution of the intact mRNA-LNP as well as the redistribution of its constituents and metabolites to evaluate the immunogenic potential of the intact mRNA-LNP formulation, its constituents, and their metabolites.

Studies investigating mRNA-LNP biodistribution have traditionally used methods such as intracellular enzymatic reporters to track the delivery of intact encapsulated mRNA into host cells (Hassett et al., 2019; Aldosari et al., 2021; Delehedde et al., 2021; Yang et al., 2021). Such methods provide information on the biodistribution of intact mRNA-LNPs, but because the reporting capacity of these techniques is dependent solely on the viability and successful delivery of the intact mRNA, this method has limited use in determining the in vivo fates of constituents, metabolites, or of damaged mRNA-LNPs (Blakney et al., 2019). To address the limitations

Downloaded from dmd.aspetjournals.org at ASPET Journals on April 20, 2024

DMD Fast Forward. Published on May 19, 2023 as DOI: 10.1124/dmd.122.000980
This article has not been copyedited and formatted. The final version may differ from this version.

associated with conventional LNP biodistribution studies, we evaluated the distribution of Heptadecane-9-yl 8-((2-hydroxyethyl)(8-(nonyloxy)-8-oxooctyl)amino)octanoate (Lipid 5), a xenobiotic amino lipid comprising a slightly polar head group and aliphatic lipid tail; Lipid 5 is distributed within the inner core of LNPs where it assists in mRNA stabilization (**Figure 1**). Analysis techniques included quantitative whole body autoradiography (QWBA) due to its capabilities allowing for assessing distribution profiles of intact and dismantled LNPs depending on the use of suitably radiolabeled constituents. This analysis method in combination with traditional metabolism and elimination studies provide an overview of the physiological fates of Lipid 5 and lipid 5-containing LNPs. QWBA analyses were performed in male and female rats after intravenous (IV) administration of radiolabeled Lipid 5 ([^{14}C]Lipid 5)-containing LNPs encapsulating non-translating factor IX (NTFIX) mRNA. This report includes the results of QWBA performed to assess the distribution of Lipid 5 and its ^{14}C-containing metabolites ([^{14}C]metabolites) after IV administration of the same NTFIX mRNA-encapsulating, [^{14}C]Lipid 5-containing LNP as well traditional assessments of lipid, mRNA, and expressed protein from an IV administered therapeutic LNP of similar lipid composition that encapsulates a similarly sized mRNAs. The ability of QWBA to track both intact [^{14}C]Lipid 5 and its [^{14}C]metabolites provides a detailed understanding of the in vivo distribution and persistence of Lipid 5-derived compounds, makes it complementary to standard LC-MS/MS techniques used for biodistribution studies in LNP component in vivo fate assessments. In addition, this study assessed the impact of endogenous pigmentation (i.e., melanin; (Solon, 2015) on the biodistribution profiles of Lipid 5 and its radiolabeled metabolites in pigmented (Long-Evans) and nonpigmented (Sprague Dawley) rats. Details regarding Lipid 5 metabolism and elimination following IV administration in male and female rats will be reported separately (Burdette et al., manuscript in preparation).

Downloaded from dmd.aspetjournals.org at ASPET Journals on April 20, 2024

DMD Fast Forward. Published on May 19, 2023 as DOI: 10.1124/dmd.122.000980
This article has not been copyedited and formatted. The final version may differ from this version.

MATERIALS AND METHODS

Reagents and Materials. All chemicals used were of reagent grade unless stated otherwise. Lipid 5 was synthesized as previously described (Sabnis et al., 2018) and labelled with ^{14}C at the proximal carbon of the ethanolamine aliphatic chain linked to the tertiary nitrogen (Eurofins; Columbia, MO; **Figure 1**). The radiolabeled site was selected as it was identified to be the most protected from known ester hydrolysis and β-oxidation degradation pathways for Lipid 5 (Burdette et al., manuscript in preparation). The purity of Lipid 5 and [^{14}C]Lipid 5 were determined as 95% chemical purity and 99% radiochemical purity, respectively.

mRNA and LNP production. Complete N1-methylpseudouridine-substituted mRNA was synthesized *in vitro* from a linearized DNA template containing the 5′ untranslated region, the 3′ untranslated region, and a poly-A tail, as described previously (Sabnis et al., 2018). After purification, mRNA (NTFIX for [^{14}C]Lipid 5-containing LNPs and similarly sized mRNA for Lipid 5-containing LNPs) was diluted in citrate buffer (Teknova) and frozen for subsequent use. LNP formulations were prepared by ethanol drop nanoprecipitation as described previously (Sabnis et al., 2018). In short, Lipid 5 or [^{14}C]Lipid 5, dipalmitoylphosphatidylcholine, cholesterol, and PEGylated lipid (CordenPharma) were dissolved in ethanol (Merck KGaA) and combined with acidified mRNA at a ratio of 3:1 (aqueous:ethanol). The product was diluted in citrate-buffered saline, maintained, and combined with a Tris buffer (pH 7.75) followed by a matched buffered excipient solution. The resulting formulation was filtered through an 0.8/0.2-μm filter (Pall Corporation), buffer exchanged into sucrose containing Tris buffer (pH 7.4), and concentrated using tangential flow filtration. Both radiolabeled and non-radiolabeled LNPs had similar lipid composition, size (60-120 nm), storage and serum stability regardless of encapsulated mRNA (dynamic light scattering on a DynaPro Plate Reader [Wyatt; Goleta, CA]).

Downloaded from dmd.aspetjournals.org at ASPET Journals on April 20, 2024

DMD Fast Forward. Published on May 19, 2023 as DOI: 10.1124/dmd.122.000980
This article has not been copyedited and formatted. The final version may differ from this version.

The Lipid 5 content of the radiolabeled LNPs included 7.5% [^{14}C]Lipid 5. The mRNA concentration and encapsulation were measured via a RiboGreen fluorescence assay (Thermo Fisher Scientific) and specific activity was measured via liquid scintillation. The formulation was stored at -80°C.

Intravenous Administration of [^{14}C]Lipid 5-containing mRNA-LNP to rats. Sprague Dawley (SD; 5 males and 5 females) or Long-Evans (LE; 5 males and 5 females) rats were intravenously administered 2 mg/kg [^{14}C]Lipid 5-containing LNP encapsulating a single, nontranslating mRNA (NTFIX; Eurofins) over a 10-minute period (35 uCi dosed per animal). One male and 1 female SD and LE rat were euthanized at 1, 10, 24, 48, and 168 hours postdose to assess [^{14}C]Lipid 5 biodistribution from peak systemic exposure to near complete systemic clearance based on previous experiments. Animals were euthanized via carbon dioxide anesthetic (7-liter chamber flushed with CO_2 [99.9% purity] at a 3-L/min flow rate with 42.8% volume displacement) and immersed in a hexane/dry ice bath for approximately 6 to 11 minutes. Animal carcasses were drained, blotted dry, embedded in 5% carboxymethylcellulose (CMC; Sigma-Aldrich), and stored at -10 to -30°C until further use. All research involving animals was conducted at Charles River Laboratories (CRL) in accordance with CR-Mattawan and Moderna, Inc. Animal Care and Use Committee guidelines.

QWBA analysis. Prior to sectioning, frozen standards comprising CMC and food coloring (N ≥4) were used so as to ensure section thickness quality control. Frozen, embedded rat carcasses were sectioned in approximately 30 μm slices through the sagittal plane and captured on adhesive tape. Sections that displayed optimal visibility of tissues and biological fluids of interest were scanned subsequent to exposure to phosphor imaging screens. Scans were quantified by using image densitometry (MCID Image Analysis software version 7.1) and standardized to

Downloaded from dmd.aspetjournals.org at ASPET Journals on April 20, 2024

DMD Fast Forward. Published on May 19, 2023 as DOI: 10.1124/dmd.122.000980
This article has not been copyedited and formatted. The final version may differ from this version.

calibration controls; a standard curve was constructed from the integrated response (MDC/mm^2) and ^{14}C calibration standard concentrations. A lower limit of quantification of 40-ng equivalents/g was established based on radioactivity measured from the lowest calibration standard used divided by the specific activity of the dose formulation (μCi/μg). Artifacts were excluded as necessary from the analysis during image processing.

Administration of Nonradioactive LNPs to rats. Thirty male and 30 female SD rats were administered Lipid 5-containing LNPs encapsulating a different, similarly sized, mRNA than NTFIX (2 mg/kg) via intravenous injection; blood and tissue samples were collected at 0, 0.16, 1, 4, 10, 24, 48, 72, 120, and 168 hour time points after administration (n=6; 3 males and 3 females) to be able to fully characterize the biodistribution and pharmacokinetics of Lipid 5, mRNA, and protein components. Animals were euthanized via carbon dioxide inhalation followed by whole-body perfusion with phosphate-buffered saline (PBS)-perfusate-containing heparin (0.9% NaCl, heparin (1000 IU/L), 1% $NaNO_3$; reconstituted in 1X PBS). Perfusion was performed until the solution draining the atrium was considered clear by visual inspection. Rat liver, spleen, lymph nodes (axillary, inguinal, and popliteal lymph nodes), lung, jejunum, stomach, kidney, heart, testes, muscle, thymus, eye, brain, ovaries, uterus, bone marrow (femur) and plasma were collected.

Quantification of Lipid 5 by liquid chromatography–tandem mass spectrometry. Quantification of Lipid 5-containing rat blood samples was determined via high-performance LC (HPLC) coupled with LC-MS/MS and validated as per FDA Bioanalytical Method Validation guidelines for industry (FDA, 2018). For the analysis of rat tissue samples, a qualification of analytical method was performed via accuracy and precision, selectivity, and recovery of Lipid 5

Downloaded from dmd.aspetjournals.org at ASPET Journals on April 20, 2024

DMD Fast Forward. Published on May 19, 2023 as DOI: 10.1124/dmd.122.000980
This article has not been copyedited and formatted. The final version may differ from this version.

in brain, heart, liver, spleen, lung, kidney, stomach, small intestine, bone marrow, testes, skeletal muscle, ovaries, uterus, full thickness tail skin, eyes, thymus, jugular vein, and lymph node tissue homogenates. Tissue homogenate samples were prepared by suspending 200 mg tissue in 4% bovine serum albumin followed by bead homogenization. Resulting homogenates underwent acetonitrile:methanol (1:1) protein precipitation and centrifugation at 4,000 rpm for 10 minutes at 5°C, and the resulting supernatant was used for further analysis. Samples were analyzed via reverse-phase (C8) LC on an Agilent 1200 HP liquid chromatograph coupled with a Sciex Triple Quad API 5000 LC-MS/MS system. The MS/MS was operated at positive-ion polarity and multiple-reaction-monitoring scanning mode; acquisitions of Lipid 5-specific signals were identified via 710.7 m/z- to >472.5 m/z-specific transition. Concentrations of Lipid 5 were determined via linear regression of a Lipid 5 calibration curve (0.5 to 500 ng/mL); the lower limit of quantification (LLOQ) of Lipid 5 in plasma and tissues was 0.500 ng/mL. A 95% mean recovery of Lipid 5 from tissues was observed as evaluated with low and high quality control standards.

Quantification of mRNA by bDNA assay. mRNA quantification in rats administered mRNA-LNPs was performed using a QuantiGene 2.0 kit (Thermo Fisher Scientific). Rat plasma and homogenized tissue samples were collected and lysed prior to analysis. Calibration standards and quality control samples were prepared in both pooled sera and pooled tissue homogenates and processed similarly to tissue samples. All resulting samples underwent a minimum 100-fold dilution in lysis buffer (Thermo Fisher Scientific) prior to conducting of branched DNA assay. Coated plates were exposed to the diluted rat samples overnight at 55°C, washed, exposed to a pre-AMP working solution for 1 hour at 55°C, and to a label probe working solution for 1 hour

Downloaded from dmd.aspetjournals.org at ASPET Journals on April 20, 2024

DMD Fast Forward. Published on May 19, 2023 as DOI: 10.1124/dmd.122.000980
This article has not been copyedited and formatted. The final version may differ from this version.

at 50°C. The resulting plate was washed, and the quality control 2.0 substrate added to each well, which was incubated for 5 minutes at room temperature. Data acquisition was performed using a Spectramax luminometer (Molecular Devices), captured on Softmax PRO Gxp software (Molecular Devices; version 5.4.6) and further analyzed using Watson LIMS (Thermo Fisher Scientific; version 7.6.1 HF1). The LLOQ of mRNA in plasma and tissues were 0.0466 ng/mL and 0.466 ng/mL, respectively.

Quantification of protein by LC-MS/MS. Quantification of translated protein product in rats administered Lipid 5-containing mRNA-LNPs were performed via LC-MS/MS. Rat tissue samples were homogenized in T-PER (Thermo Fisher Scientific), reduced with 2 µL of 100 mM TCEP, and denatured by incubating at 100°C for 10 minutes. The samples were then cooled to room temperature and alkylated by adding 4 µL of 50 mM iodoacetamide. Subsequent protein digestion was performed by exposing the alkylated sample to a trypsin solution (0.2 µg/µL) at a final ratio of 1:20 (trypsin:protein) at 45°C for 1 hour. Resulting digested samples were centrifuged at 14,000 rpm (18,407 xg) for 10 min, and the supernatant combined with an isotopically labeled internal standard. Samples were analyzed using a Triple Quad API 7500 MS system (Sciex). The LLOQ of protein in tissues was 20.0 pg/mL.

PK and PD analysis. Pharmacokinetic parameters (mRNA and Lipid 5) and pharmacodynamic parameters (protein) were calculated using noncompartmental analysis (Phoenix WinNonlin version 8.3).

RESULTS

Biodistribution of [^{14}C]Lipid 5 and its ^{14}C-containing metabolites in SD and LE rats.

Downloaded from dmd.aspetjournals.org at ASPET Journals on April 20, 2024

DMD Fast Forward. Published on May 19, 2023 as DOI: 10.1124/dmd.122.000980
This article has not been copyedited and formatted. The final version may differ from this version.

Radioactivity appeared rapidly, with maximal concentrations measured in several tissues within the first hour after administration of [^{14}C]Lipid 5-containing LNPs (**Figure 2A** and **Supplementary Figure 1**). In SD rats, the liver (20,000 ng equivalents test article/g), adrenal gland (12,000 ng equivalents test article/g), spleen (8320 ng equivalents test article/g), and small-intestinal contents (6800 ng equivalents test article/g) had the highest distributions of radioactivity compared with other tissues at 1 hour (**Figure 3**). By 10 hours (**Figure 2B** and **Supplementary Figure 2**), a general decrease in radioactivity was observed throughout most tissues compared with the 1 hour time point, with the maximum distribution observed within the large-intestinal contents (14,500 ng equivalents test article/g), cecum contents (7,530 ng equivalents test article/g), urine (7,990 ng equivalents test article/g), and liver (3,880 ng equivalents test article/g) for both male and female rats (**Figure 3**). By the 24 hour time point (**Supplementary Figure 3**), the majority of the radioactivity had been eliminated from the animals of both sexes, with the large-intestinal contents (4550 ng equivalents test article/g), cecum contents (1230 ng equivalents test article/g), small-intestinal contents (930 ng equivalents test article/g), and liver (892 ng equivalents test article/g) displaying modest to medium levels of radioactivity in both male and female rats compared with both the 1 hour and 10 hour time points (**Figure 3; Supplementary Tables 1** and **2**). Through 48 hours (**Supplementary Figure 4**) and 168 hours (**Figure 2C** and **Supplementary Figure 5**), radioactivity measurements were low or indistinguishable from background in most tissues; minimal levels of radioactivity were measured in the small-intestinal contents (284 ng equivalents test article/g), liver (227 ng equivalents test article/g), and large-intestinal contents (192 ng equivalents test article/g) at 48 hours, with negligible amounts detected in the adrenal gland (139 ng equivalents test article/g), spleen (71 ng equivalents test article/g), and liver (59 ng equivalents test article/g) at 168 hours

Downloaded from dmd.aspetjournals.org at ASPET Journals on April 20, 2024

DMD Fast Forward. Published on May 19, 2023 as DOI: 10.1124/dmd.122.000980
This article has not been copyedited and formatted. The final version may differ from this version.

for both male and female rats. Detectable amounts of radioactivity were measured in the ovaries of female rats at 48 and 168 hours (225 and 169 ng equivalents test article/g, respectively) while levels were undetectable in testes at the same timepoints. The biodistribution of Lipid 5 and [^{14}C]metabolites) were similar between SD and LE rats at all time points assessed (**Supplementary Figures 6–10** and **Supplementary Tables 3** and **4**), including having comparable distribution between pigmented and nonpigmented tissue for most time points.

Biodistribution of Lipid 5, mRNA, and protein products in SD rats using a therapeutic mRNA-LNP. Rapid biodistribution of intact Lipid 5 was seen in most tissues, achieving maximum observed concentration (T_{max}) at the earliest time tested (0.16 hours) (**Table 1**; **Figure 4**) with only the liver (**Figure 4B**) and spleen (**Figure 4G**) reaching T_{max} levels at 1 hour post dose. The highest Lipid 5 tissue concentrations (C_{max}) were recorded in the plasma (54,700 ± 12,800 ng/mL; **Figure 4A**), followed by the lungs (14,600 ± 2450 ng/g; **Figure 4H**), kidney (9410 ± 2640 ng/g; **Figure 4C**), and liver (8050 ± 846 ng/g; Figure 3B) as compared with other tissues. The highest areas under the curve (AUC_{last}) values observed for Lipid 5 were in the plasma and spleen, at 85,700 ± 14,800 hour*ng/mL and 26,900 ± 2120 hour*ng/g, respectively, followed by the liver, lungs, and kidney at 25,400 ± 2060 hour*ng/g, 21,000 ± 3660 hour*ng/g, and 10,100 ± 1460 hour*ng/g, respectively. Total tissue distribution as it relates to plasma (tissue-to-plasma AUC ratio) was measured maximally, at 31.4%, 29.6%, 24.5%, and 11.8%, for the spleen, liver, lungs, and kidney, respectively; and to a lesser extent, within the jejunum, stomach, testes, heart, thymus, uterus, brain, and muscle in descending order of distribution levels (**Table 1**). Insufficient data were available for accurate determination of pooled lymph nodes, eye, ovary, and femur bone marrow exposure profiles. By 168 hours, most tissues were

Downloaded from dmd.aspetjournals.org at ASPET Journals on April 20, 2024

DMD Fast Forward. Published on May 19, 2023 as DOI: 10.1124/dmd.122.000980
This article has not been copyedited and formatted. The final version may differ from this version.

completely cleared of Lipid 5, with the longest half-life ($T_{1/2}$) of Lipid 5 reported in the lungs at 23.1 hours; the $T_{1/2}$ in liver was 9.30 hours.

In the evaluation of the distribution of the LNP mRNA component **(Table 2; Figure 5)**, T_{max} was reported within 1 hour for the majority of tissues, with the jejunum (**Figure 5B**) and eyes (**Figure 5E**) reaching T_{max} at 4 hours, and the axillary and inguinal lymph nodes (**Figure 5G**) reaching T_{max} at 48 hours. The highest mRNA distribution (C_{max}) occurred in plasma (18,200 ± 3450 ng/mL; **Figure 5A**), liver (8530 ± 1340 ng/g; **Figure 5B**), lungs (4500 ± 1070 ng/g; **Figure 5H**), and spleen (3030 ± 1130 ng/g; **Figure 5G**) compared with other tissues examined. The highest AUC_{last} values were also reported in the spleen (202,000 ± 21,400 hour*ng/g), plasma (146,000 ± 14,600 hour*ng/mL), liver (34,000 ± 3340 hour*ng/g), and lungs (18,900 ± 2040 hour*ng/g). Compared with all tissues, the spleen showed the greatest tissue-to-plasma ratio, at 138%, followed by the liver at 23.3% and the lungs at 12.9%, with the remaining tissues at a less than 6.05% tissue-to-plasma ratio (including the kidney, heart, muscle, jejunum, testes, stomach, thymus, uterus, brain, femur, and brain marrow in descending order of ratios; **Table 2**). Insufficient data were available to accurately determine axillary and popliteal lymph node, eye, and ovary AUC values. Half-life values ranged from 4.76 to 55.1 hours in all tissues where estimable. The spleen (**Figure 5G**) had the longest calculated $T_{1/2}$ values, of 55.1 hours, among all tissues examined; the $T_{1/2}$ of mRNA in liver was 8.15 hours.

Protein expressed from LNP-encapsulated mRNA **(Table 3; Figure 6)** was rapidly detected in the thymus (TE_{max} of 0.83 hour; **Figure 6G**), while the uterus (**Figure 6F**) and kidneys (**Figure 6C**) only reached TE_{max} at 72 hours. The highest E_{max} was observed in the liver (44.2 ± 7.06 µg/g; **Figure 6B**) and ovaries (14.7 µg/g; **Figure 6F**) compared with the other tissues examined. Protein AUEC values were highest in the liver (1,520 ± 157 hour*µg/g; **Figure 6B**), and kidney

Downloaded from dmd.aspetjournals.org at ASPET Journals on April 20, 2024

DMD Fast Forward. Published on May 19, 2023 as DOI: 10.1124/dmd.122.000980
This article has not been copyedited and formatted. The final version may differ from this version.

(72.1 ± 23.0 hour*µg/g; **Figure 6C**) followed by the lung, jejunum, heart, thymus, spleen, uterus, stomach, testes, and brain in descending order of protein levels (**Table 3**). Insufficient data were available to accurately determine ovary, muscle, femur bone marrow, eye, and pooled lymph node AUEC exposure profiles. Protein was detected for at least 72 hours in the majority of tissues, and the longest half-life for protein was observed in the lungs, at 121 hours. The protein $T_{1/2}$ in liver was 35.3 hours.

Downloaded from dmd.aspetjournals.org at ASPET Journals on April 20, 2024

DMD Fast Forward. Published on May 19, 2023 as DOI: 10.1124/dmd.122.000980
This article has not been copyedited and formatted. The final version may differ from this version.

DISCUSSION

The technology behind mRNA-based medicines has developed rapidly over the last decade and, in the face of the COVID-19 pandemic, mRNA medicines have demonstrated their safety and effectiveness as vaccines (Polack et al., 2020; Baden et al., 2021). While there now exists a greater understanding regarding the utility of mRNA-based medicines, the biodistribution profiles of LNPs and their constituents as well as the drivers influencing their biodistribution are less well understood. With the development of novel therapeutic and prophylactic mRNA-LNP modalities, many of which incorporate xenobiotic constituents, an in-depth biodistribution profile analysis is necessary to understand the *in vivo* fates and factors that influence the *in vivo* exposure of these medicines and their constituents. These data will inform the evolving clinical evaluation strategy as well as providing insight into future mRNA-LNP product development. In this study, we showed that after IV administration of Lipid 5, a xenobiotic amino lipid used in LNP formulations, rapidly distributes throughout rat tissues *in vivo*, with exposure directed primarily toward the liver, spleen, lung, and kidneys. In addition, we showed that Lipid 5 and its [^{14}C]metabolites are undetectable in most tissues within 7 days (168 hours). Our findings showed similar distribution profiles in both male and female, pigmented and nonpigmented rats, suggesting minimal influence of sex or pigmentation in exposure of Lipid 5 and its [^{14}C]metabolites. The findings support the use of non-radioactive analyses in rat biodistribution models to assess the efficacy and safety of Lipid 5-containing LNPs in a preclinical setting.

The tissue distribution analysis using [^{14}C]Lipid 5-containing LNPs showed rapid distribution of Lipid 5 and its [^{14}C]metabolites throughout all tissues tested within the first hour, localizing primarily in the digestive and urinary systems (**Figure 2 and 3**). Ten hours after IV LNP administration, the majority of the remaining radioactivity was eliminated from the peripheral

Downloaded from dmd.aspetjournals.org at ASPET Journals on April 20, 2024

DMD Fast Forward. Published on May 19, 2023 as DOI: 10.1124/dmd.122.000980
This article has not been copyedited and formatted. The final version may differ from this version.

tissues and was concentrated primarily in the digestive system (intestines, intestinal lumen, and other organs that facilitate metabolism and excretion of xenobiotics such as the liver (Kok-Yong and Lawrence, 2015). Notably, the levels observed at the 10-hour timepoint were much lower than that of the same tissues 1 hour after the [^{14}C]Lipid 5-containing LNP was administered. By 24 hours, the majority of radioactivity was exclusively distributed within the digestive system, with minimal ^{14}C detected in other organ systems. The localization and progression over time of ^{14}C in the liver, small intestine, and large intestine is suggestive of hepatobiliary clearance with [^{14}C]Lipid 5 and its [^{14}C]metabolites excreted into bile and eliminated via feces (Kok-Yong and Lawrence, 2015); this predicted clearance pathway is similar to previous studies examining LNP clearance using fluorescent-dye-labeled LNPs (Press et al., 2014). The localization of ^{14}C in the kidneys and intra-bladder urine is also consistent with observation from other studies where the majority of radioactivity (62%) from labelled Lipid 5-containing LNPs administered to SD rats were excreted through urine, primarily as oxidative metabolites produced via ester hydrolysis and β-oxidation of Lipid 5 (Burdette et al., manuscript in preparation). Excluding the digestive and urinary system, other organs with high observed levels of radioactivity were the adrenal glands, lungs, spleen, and lymph nodes, which were consistent with biodistribution profiles previously reported for RNA encapsulating LNPs (Chen et al., 2019; EMA, 2021; Di et al., 2022). In female SD and LE rats, high concentrations of Lipid 5 were observed in the ovaries, but with insufficient duration of exposure to calculate an AUC. This observed exposure could potentially be attributed to accumulation within the cumulus cell layers surrounding the oocytes, as has been reported for nanoparticle delivery systems previously (Hou and Zhu, 2017); however, detailed analysis is needed to confirm that hypothesis. Excluding reproductive organs, similar trends in ^{14}C biodistribution were observed between male and female rats, with

Downloaded from dmd.aspetjournals.org at ASPET Journals on April 20, 2024

DMD Fast Forward. Published on May 19, 2023 as DOI: 10.1124/dmd.122.000980
This article has not been copyedited and formatted. The final version may differ from this version.

differences primarily occurring within the first 10 hours after administration of the LNPs. The study did not find high or increasing concentrations of ^{14}C in non-excretory systems post initial administration in male and female SD and LE rats, which suggests that both [^{14}C]Lipid 5 and its [^{14}C]metabolites are rapidly eliminated rather than extensively redistributed throughout the body, consistent with observations from other studies (Caldwell et al., 1995). The lack of an observed difference in ^{14}C biodistribution between pigmented (LE) and nonpigmented (SD) rats suggests a minimal influence of endogenous pigmentation such as melanin on intravenously administered Lipid 5 exposure. These findings are expected to be translatable to Lipid 5-containing LNP *in vivo* exposure studies in other animal species.

Biodistribution analysis of Lipid 5 by using LC-MS/MS was consistent with biodistributions from the QWBA studies. Lipid 5 and mRNA exposure after administration of mRNA-LNPs concentrated primarily within the plasma, liver, spleen, lungs, and kidney, with the most rapid clearance occurring in the plasma, The longest duration of exposure was in the spleen, consistent with previous reports for mRNA-encapsulating LNPs (Lee et al., 2010; Bahl et al., 2017). As described previously, the differential tissue uptake of intact LNPs into cells in combination with dissimilar tissue perfusion rates may provide an explanation for the observed inter-tissue exposure and timing differences (Currie, 2018). Also, the delay between peak protein expression (**Table 3** and **Figure 6**) and peak Lipid 5 (**Table 1** and **Figure 4**) and mRNA exposure (**Table 2** and **Figure 5**) is consistent with the necessity for cellular uptake and endosomal release prior to target protein translation (Alfagih et al., 2020). Although these may be plausible explanations for the observations made, additional research is needed to test these mechanistic hypotheses.

Both QWBA and LC-MS/MS analyses performed on similar LNPs encapsulating different mRNAs, showed comparable biodistribution profiles for Lipid 5, even with QWBA analyses also

Downloaded from dmd.aspetjournals.org at ASPET Journals on April 20, 2024

DMD Fast Forward. Published on May 19, 2023 as DOI: 10.1124/dmd.122.000980
This article has not been copyedited and formatted. The final version may differ from this version.

including the presence of [^{14}C]metabolites. This demonstrates the applicability of standard non-radioactive methods for assessing LNP and LNP component tissue distribution for Lipid 5-containing LNPs. Since QWBA allows for the quantification of labelled parent molecules and metabolites (Solon and Kraus, 2001), the similarities observed between QWBA (Lipid 5 and its [^{14}C]metabolites) and LC-MS/MS analysis (intact Lipid 5 only) suggest that [^{14}C]metabolite distribution and persistence in tissues do not differ greatly from that of the parent Lipid 5. Additionally, increasing concentrations of [^{14}C]Lipid 5 and its [^{14}C]metabolites were not observed following the initial increase post administration, suggesting that redistribution of the xenobiotic lipid, and its [^{14}C]metabolites, is not expected. This study also reported similar biodistribution profiles for two different mRNA constructs of similar sizes encapsulated into LNPs with the same lipid constituents, suggesting that the LNP composition rather than the mRNA component is primarily responsible for the biodistribution profile of these mRNA-LNPs. The different mRNA-LNPs delivered support the extrapolation of findings to other mRNA-LNPs of similar morphology and composition. However, this may differ for mRNA-LNPs of other sizes, surface charge, lipid composition, or surface modifications such as antibodies, receptors, or ligands.

The modest sample size used for QWBA analyses, with only two animals (1 male and 1 female), assessed for each time point, is in alignment with the industry standard while also minimizing the use of study animals (Solon and Kraus, 2001). Regardless, consistency in the data obtained between individuals supports the robustness of the study design to investigate the in vivo analysis of Lipid 5-containing LNPs. This study contributes to the interpretation and design of preclinical pharmacology and toxicology studies with the potential of extrapolating findings for clinical study considerations (European Medicines Agency, 2021). The extrapolations are

Downloaded from dmd.aspetjournals.org at ASPET Journals on April 20, 2024

DMD Fast Forward. Published on May 19, 2023 as DOI: 10.1124/dmd.122.000980
This article has not been copyedited and formatted. The final version may differ from this version.

supported by established pharmacology and toxicology mechanisms that are shared between rodents and humans (European Medicines Agency, 2021). The similar Lipid 5 biodistribution profiles observed, regardless of pigmentation or sex, and lack of evidence of redistribution of LNP-derived Lipid 5 or its [^{14}C]metabolites demonstrates that the biodistribution strategy used within this study provides a clear understanding of systemic exposure, and thus informs Lipid 5-based LNP clinical safety and drug-drug interactions (DDI). The rapid elimination of all Lipid 5-derived radioactivity from the body in combination with the mechanistic understanding of metabolism and clearance via multiple, ubiquitous, high-capacity systems as detailed in previous studies (Sabnis et al., 2018; Burdette et al., manuscript in preparation). These findings in combination with traditional cytochrome P450s enzyme superfamilies and drug transporter studies (Ci et al., manuscript in preparation) support the overall, low probability of DDI with co-administered medications and thus informs the continued use of Lipid 5 therapeutic LNPs.

The results from this study demonstrate that Lipid 5-containing LNPs are distributed throughout tissues after initial IV administration and Lipid 5 is rapidly eliminated thereafter. The time course and radioactivity distribution patterns of [^{14}C]Lipid 5-containing LNPs, suggest that Lipid 5 and its [^{14}C]metabolites undergo elimination by both biliary and renal routes with no indication of redistribution or prolonged metabolite exposure. Furthermore, biodistribution profiles were consistent between pigmented and nonpigmented male and female rats, indicating that neither sex nor pigmentation influences Lipid 5 exposure. The findings of this *in vivo* preclinical study support the translatability of Lipid 5 exposure profiles in standard rat biodistribution studies to humans as a complement to appropriately designed safety studies due to shared absorption, distribution, metabolism, and excretion pathways.

Downloaded from dmd.aspetjournals.org at ASPET Journals on April 20, 2024

DMD Fast Forward. Published on May 19, 2023 as DOI: 10.1124/dmd.122.000980
This article has not been copyedited and formatted. The final version may differ from this version.

REFERENCES

Aldosari BN, Alfagih IM, and Almurshedi AS (2021) Lipid Nanoparticles as Delivery Systems for RNA-Based Vaccines. *Pharmaceutics* **13**.

Alfagih IM, Aldosari B, AlQuadeib B, Almurshedi A, and Alfagih MM (2020) Nanoparticles as Adjuvants and Nanodelivery Systems for mRNA-Based Vaccines. *Pharmaceutics* **13**.

Baden LR, El Sahly HM, Essink B, Kotloff K, Frey S, Novak R, Diemert D, Spector SA, Rouphael N, Creech CB, McGettigan J, Khetan S, Segall N, Solis J, Brosz A, Fierro C, Schwartz H, Neuzil K, Corey L, Gilbert P, Janes H, Follmann D, Marovich M, Mascola J, Polakowski L, Ledgerwood J, Graham BS, Bennett H, Pajon R, Knightly C, Leav B, Deng W, Zhou H, Han S, Ivarsson M, Miller J, Zaks T, and Group CS (2021) Efficacy and Safety of the mRNA-1273 SARS-CoV-2 Vaccine. *N Engl J Med* **384:**403-416.

Bahl K, Senn JJ, Yuzhakov O, Bulychev A, Brito LA, Hassett KJ, Laska ME, Smith M, Almarsson O, Thompson J, Ribeiro AM, Watson M, Zaks T, and Ciaramella G (2017) Preclinical and Clinical Demonstration of Immunogenicity by mRNA Vaccines against H10N8 and H7N9 Influenza Viruses. *Mol Ther* **25:**1316-1327.

Blakney AK, McKay PF, Yus BI, Aldon Y, and Shattock RJ (2019) Inside out: optimization of lipid nanoparticle formulations for exterior complexation and in vivo delivery of saRNA. *Gene Ther* **26:**363-372.

Caldwell J, Gardner I, and Swales N (1995) An introduction to drug disposition: the basic principles of absorption, distribution, metabolism, and excretion. *Toxicol Pathol* **23:**102-114.

Chan CL, Majzoub RN, Shirazi RS, Ewert KK, Chen YJ, Liang KS, and Safinya CR (2012) Endosomal escape and transfection efficiency of PEGylated cationic liposome-DNA complexes prepared with an acid-labile PEG-lipid. *Biomaterials* **33:**4928-4935.

Chen D, Parayath N, Ganesh S, Wang W, and Amiji M (2019) The role of apolipoprotein- and vitronectin-enriched protein corona on lipid nanoparticles for in vivo targeted delivery

Downloaded from dmd.aspetjournals.org at ASPET Journals on April 20, 2024

DMD Fast Forward. Published on May 19, 2023 as DOI: 10.1124/dmd.122.000980
This article has not been copyedited and formatted. The final version may differ from this version.

and transfection of oligonucleotides in murine tumor models. *Nanoscale* **11:**18806-18824.

Currie GM (2018) Pharmacology, Part 2: Introduction to Pharmacokinetics. *J Nucl Med Technol* **46:**221-230.

Damase TR, Sukhovershin R, Boada C, Taraballi F, Pettigrew RI, and Cooke JP (2021) The Limitless Future of RNA Therapeutics. *Front Bioeng Biotechnol* **9:**628137.

Delehedde C, Even L, Midoux P, Pichon C, and Perche F (2021) Intracellular Routing and Recognition of Lipid-Based mRNA Nanoparticles. *Pharmaceutics* **13**.

Di J, Du Z, Wu K, Jin S, Wang X, Li T, and Xu Y (2022) Biodistribution and Non-linear Gene Expression of mRNA LNPs Affected by Delivery Route and Particle Size. *Pharm Res*.

EMA (2021) Assessment report: Comirnaty. https://www.ema.europa.eu/en/documents/assessment-report/comirnaty-epar-public-assessment-report_en.pdf. Date accessed 22 Apr 2022.

European Medicines Agency (2021) Nonclinical biodistribution considerations for gene therapy products S12.

FDA (2018) Bioanalytical Method Validation Guidance for Industry.

Guevara ML, Persano F, and Persano S (2020) Advances in Lipid Nanoparticles for mRNA-Based Cancer Immunotherapy. *Front Chem* **8:**589959.

Hassett KJ, Benenato KE, Jacquinet E, Lee A, Woods A, Yuzhakov O, Himansu S, Deterling J, Geilich BM, Ketova T, Mihai C, Lynn A, McFadyen I, Moore MJ, Senn JJ, Stanton MG, Almarsson O, Ciaramella G, and Brito LA (2019) Optimization of Lipid Nanoparticles for Intramuscular Administration of mRNA Vaccines. *Mol Ther Nucleic Acids* **15:**1-11.

Hou CC and Zhu JQ (2017) Nanoparticles and female reproductive system: how do nanoparticles affect oogenesis and embryonic development. *Oncotarget* **8:**109799-109817.

Downloaded from dmd.aspetjournals.org at ASPET Journals on April 20, 2024

DMD Fast Forward. Published on May 19, 2023 as DOI: 10.1124/dmd.122.000980
This article has not been copyedited and formatted. The final version may differ from this version.

Hou X, Zaks T, Langer R, and Dong Y (2021) Lipid nanoparticles for mRNA delivery. *Nat Rev Mater***:**1-17.

Kalyanram P, Puri A, and Gupta A (2022) Thermotropic effects of PEGylated lipids on the stability of HPPH-encapsulated lipid nanoparticles (LNP). *J Therm Anal Calorim* **147:**6337-6348.

Kok-Yong S and Lawrence L (2015) Drug Distribution and Drug Elimination, InTech.

Lee MJ, Veiseh O, Bhattarai N, Sun C, Hansen SJ, Ditzler S, Knoblaugh S, Lee D, Ellenbogen R, Zhang M, and Olson JM (2010) Rapid pharmacokinetic and biodistribution studies using cholorotoxin-conjugated iron oxide nanoparticles: a novel non-radioactive method. *PLoS One* **5:**e9536.

Lee YK, Lee H, and Nam J-M (2013) Lipid-nanostructure hybrids and their applications in nanobiotechnology. *NPG Asia Materials* **5:**e48-e48.

Ndeupen S, Qin Z, Jacobsen S, Estanbouli H, Bouteau A, and Igyártó BZ (2021) The mRNA-LNP platform's lipid nanoparticle component used in preclinical vaccine studies is highly inflammatory. *bioRxiv: the preprint server for biology***:**2021.2003.2004.430128.

Polack FP, Thomas SJ, Kitchin N, Absalon J, Gurtman A, Lockhart S, Perez JL, Perez Marc G, Moreira ED, Zerbini C, Bailey R, Swanson KA, Roychoudhury S, Koury K, Li P, Kalina WV, Cooper D, Frenck RW, Jr., Hammitt LL, Tureci O, Nell H, Schaefer A, Unal S, Tresnan DB, Mather S, Dormitzer PR, Sahin U, Jansen KU, Gruber WC, and Group CCT (2020) Safety and Efficacy of the BNT162b2 mRNA Covid-19 Vaccine. *N Engl J Med* **383:**2603-2615.

Press AT, Traeger A, Pietsch C, Mosig A, Wagner M, Clemens MG, Jbeily N, Koch N, Gottschaldt M, Beziere N, Ermolayev V, Ntziachristos V, Popp J, Kessels MM, Qualmann B, Schubert US, and Bauer M (2014) Cell type-specific delivery of short interfering RNAs by dye-functionalised theranostic nanoparticles. *Nat Commun* **5:**5565.

Rostami E, Kashanian S, Azandaryani AH, Faramarzi H, Dolatabadi JE, and Omidfar K (2014) Drug targeting using solid lipid nanoparticles. *Chem Phys Lipids* **181:**56-61.

Downloaded from dmd.aspetjournals.org at ASPET Journals on April 20, 2024

DMD Fast Forward. Published on May 19, 2023 as DOI: 10.1124/dmd.122.000980
This article has not been copyedited and formatted. The final version may differ from this version.

Sabnis S, Kumarasinghe ES, Salerno T, Mihai C, Ketova T, Senn JJ, Lynn A, Bulychev A, McFadyen I, Chan J, Almarsson O, Stanton MG, and Benenato KE (2018) A Novel Amino Lipid Series for mRNA Delivery: Improved Endosomal Escape and Sustained Pharmacology and Safety in Non-human Primates. *Mol Ther* **26:**1509-1519.

Scioli Montoto S, Muraca G, and Ruiz ME (2020) Solid Lipid Nanoparticles for Drug Delivery: Pharmacological and Biopharmaceutical Aspects. *Frontiers in Molecular Biosciences* **7**.

Shi L, Zhang J, Zhao M, Tang S, Cheng X, Zhang W, Li W, Liu X, Peng H, and Wang Q (2021) Effects of polyethylene glycol on the surface of nanoparticles for targeted drug delivery. *Nanoscale* **13:**10748-10764.

Solon EG (2015) Autoradiography techniques and quantification of drug distribution. *Cell Tissue Res* **360:**87-107.

Solon EG and Kraus L (2001) Quantitative whole-body autoradiography in the pharmaceutical industry. Survey results on study design, methods, and regulatory compliance. *J Pharmacol Toxicol Methods* **46:**73-81.

Tombacz I, Laczko D, Shahnawaz H, Muramatsu H, Natesan A, Yadegari A, Papp TE, Alameh MG, Shuvaev V, Mui BL, Tam YK, Muzykantov V, Pardi N, Weissman D, and Parhiz H (2021) Highly efficient CD4+ T cell targeting and genetic recombination using engineered CD4+ cell-homing mRNA-LNPs. *Mol Ther* **29:**3293-3304.

Veiga N, Diesendruck Y, and Peer D (2020) Targeted lipid nanoparticles for RNA therapeutics and immunomodulation in leukocytes. *Adv Drug Deliv Rev* **159:**364-376.

Yang R, Deng Y, Huang B, Huang L, Lin A, Li Y, Wang W, Liu J, Lu S, Zhan Z, Wang Y, A R, Wang W, Niu P, Zhao L, Li S, Ma X, Zhang L, Zhang Y, Yao W, Liang X, Zhao J, Liu Z, Peng X, Li H, and Tan W (2021) A core-shell structured COVID-19 mRNA vaccine with favorable biodistribution pattern and promising immunity. *Signal Transduct Target Ther* **6:**213.

Zhang R, El-Mayta R, Murdoch TJ, Warzecha CC, Billingsley MM, Shepherd SJ, Gong N, Wang L, Wilson JM, Lee D, and Mitchell MJ (2021) Helper lipid structure influences

Downloaded from dmd.aspetjournals.org at ASPET Journals on April 20, 2024

DMD Fast Forward. Published on May 19, 2023 as DOI: 10.1124/dmd.122.000980
This article has not been copyedited and formatted. The final version may differ from this version.

protein adsorption and delivery of lipid nanoparticles to spleen and liver. *Biomater Sci* **9:**1449-1463.

Downloaded from dmd.aspetjournals.org at ASPET Journals on April 20, 2024

DMD Fast Forward. Published on May 19, 2023 as DOI: 10.1124/dmd.122.000980
This article has not been copyedited and formatted. The final version may differ from this version.

ACKNOWLEDGMENTS

Medical writing and editorial assistance were provided by Wynand van Losenoord, MSc, of MEDiSTRAVA in accordance with Good Publication Practice (GPP3) guidelines, funded by Moderna, Inc., and under the direction of the authors. We acknowledge the Moderna colleagues Kerry Benenato, Greg Mercer, Don Parsons, and John Joyal for critical logistics and insightful discussion related to this work and to the Eurofins team for generating [^{14}C] Lipid 5 LNPs.

AUTHOR CONTRIBUTIONS

Participated in research design: Ci, Hard, Kenney, Auerbach, Hendrick, Almarsson, Cheung, and Burdette

Conducted experiments: Zhang, Gandham, Hua, Wickwire, Wehrman, and Slauter.

Performed data analysis: Ci, Hard, Zhang, Gandham, Hua, Wickwire, Slauter, Mercer, and Burdette.

Wrote or contributed to the writing of the manuscript: All authors

CONFLICT OF INTEREST

LC, HZ, SG, SH, JW, AA, MK, GM, EC, and DB are employees of Moderna, Inc. and hold stock/stock options in the company; MH, TW, RS, TH, and OA have no conflicts of interest to declare.

DATA-SHARING STATEMENT

The authors declare that the data supporting the findings of this study are available within this article.

Downloaded from dmd.aspetjournals.org at ASPET Journals on April 20, 2024

DMD Fast Forward. Published on May 19, 2023 as DOI: 10.1124/dmd.122.000980
This article has not been copyedited and formatted. The final version may differ from this version.

FUNDING

This study was funded by Moderna, Inc.

Downloaded from dmd.aspetjournals.org at ASPET Journals on April 20, 2024

TABLES

Table 1. Summary of Plasma and Tissue Lipid 5 Pharmacokinetic Parameters in Sprague Dawley Rats

Matrix	Median T_{max}[a] (hour)	Mean C_{max}[b] ± SE (ng/mL)	Mean AUC_{last}[c] ± SE (hour*ng/mL)	Median T_{last}[d] (hour)	Mean $T_{1/2}$[e] (hour)	Tissue-to-Plasma AUC Ratio (%)
Circulatory System						
Heart	0.16	1250 ± 385	1670 ± 244	24	3.66	1.95
Plasma	0.16	54,700 ± 12,800	85,700 ± 14,800	120	NA	100
Digestive System						
Liver	0.83	8050 ± 846	25,400 ± 2060	72	9.30	29.6
Jejunum	0.16	914 ± 296	4440 ± 999	72	17.9	5.18
Stomach	0.16	2160 ± 672	3000 ± 571	120	NA	3.50

Downloaded from dmd.aspetjournals.org at ASPET Journals on April 20, 2024

DMD Fast Forward. Published on May 19, 2023 as DOI: 10.1124/dmd.122.000980
This article has not been copyedited and formatted. The final version may differ from this version.

Urinary System						
Kidney	0.16	9410 ± 2640	10,100 ± 1460	48	6.09	11.8
Musculoskeletal System						
Skeletal Muscle	0.16	1170 ± 495	871 ± 218	10	1.82	1.02
Nervous System						
Brain	0.16	590 ± 85.4	948 ± 84.2	24	6.58	1.11
Reproductive System						
Testes	0.16	660 ± 375	2230 ± 236	72	13.9	2.60
Uterus	0.16	425 ± 293	1070 ± 525	24	4.27	1.25
Immune System						
Lymph Node: Axillary	NA	NA	NA	NA	NA	NA

Downloaded from dmd.aspetjournals.org at ASPET Journals on April 20, 2024

DMD Fast Forward. Published on May 19, 2023 as DOI: 10.1124/dmd.122.000980
This article has not been copyedited and formatted. The final version may differ from this version.

Lymph Node: Inguinal	NA	NA	NA	NA	NA	NA
Spleen	0.83	2830 ± 471	26,900 ± 2120	168	NA	31.4
Thymus	0.16	718 ± 180	1470 ± 505	10	NA	1.72
Respiratory System						
Lung	0.16	14,600 ± 2450	21,000 ± 3660	168	23.1	24.5

NA, Not applicable. Values were not obtained due to insufficient readings and/or unavailability of samples.

[a]Time to maximum observed concentration; [b]maximum observed concentration; [c]area under the concentration-versus-time curve from the start of dose administration to the last observed quantifiable concentration ; [d]time at which the last quantifiable concentration was observed; [e]elimination half-life of Lipid 5.

Downloaded from dmd.aspetjournals.org at ASPET Journals on April 20, 2024

DMD Fast Forward. Published on May 19, 2023 as DOI: 10.1124/dmd.122.000980
This article has not been copyedited and formatted. The final version may differ from this version.

Table 2. Summary Of Plasma And Tissue mRNA Pharmacokinetic Parameters In Sprague Dawley Rats

Matrix	Median T_{max}[a] (hour)	Mean C_{max}[b] ± SE (ng/mL)	Mean AUC_{last}[c] ± SE (hour*ng/mL)	Median T_{last}[d] (hour)	Mean $T_{1/2}$[e] (hour)	Tissue-to-Plasma AUC Ratio (%)
Circulatory System						
Heart	0.16	1360 ±228	6540 ± 716	48	8.97	4.48
Plasma	0.16	18,200 ± 3450	146,000 ± 14,600	72	6.26	100
Digestive System						
Liver	0.16	8530 ± 1340	34,000 ± 3340	48	8.15	23.3
Jejunum	4	97.8 ± 35.0	1970 ± 341	72	12.4	1.35
Stomach	0.16	407 ± 169	1500 ± 582	48	NA	1.03
Urinary System						

Downloaded from dmd.aspetjournals.org at ASPET Journals on April 20, 2024

DMD Fast Forward. Published on May 19, 2023 as DOI: 10.1124/dmd.122.000980
This article has not been copyedited and formatted. The final version may differ from this version.

Kidney	0.16	2340 ± 801	8830 ± 1470	168	21	6.05
Musculoskeletal System						
Skeletal Muscle	0.16	596 ± 191	2270 ± 326	48	8.08	1.56
Nervous System						
Brain	0.16	169 ± 37.4	370 ± 90.5	24	NA	0.253
Eye	4	56.4 ± 18.2	1660 ± 353	168	48.2	1.14
Reproductive System						
Testes	0.16	113 ± 50.1	1510 ± 223	48	11.2	1.03
Uterus	0.83	64.5 ± 31.9	653 ± 185	48	10	0.447
Immune System						
Lymph Node: Axillary	48	92.3	NA	120	NA	NA

Downloaded from dmd.aspetjournals.org at ASPET Journals on April 20, 2024

DMD Fast Forward. Published on May 19, 2023 as DOI: 10.1124/dmd.122.000980
This article has not been copyedited and formatted. The final version may differ from this version.

Lymph Node: Inguinal	48	184	NA	120	NA	NA
Lymph Node: Popliteal	0.16	217	NA	0.16	NA	NA
Spleen	0.83	3030 ± 1130	202,000 ± 21,400	168	55.1	138
Thymus	0.16	108 ± 32.6	1390 ± 304	168	NA	0.952
Femur Bone Marrow	0.16	3.73 ± 1.63	22.1 ± 3.58	24	4.76	0.0151
Respiratory System						
Lung	0.16	4500 ± 1070	18,900 ± 2040	168	23.5	12.9

NA, Not applicable. Values were not obtained due to insufficient readings and/or unavailability of samples.

Downloaded from dmd.aspetjournals.org at ASPET Journals on April 20, 2024

DMD Fast Forward. Published on May 19, 2023 as DOI: 10.1124/dmd.122.000980
This article has not been copyedited and formatted. The final version may differ from this version.

[a]Time to maximum observed concentration; [b]maximum observed concentration; [c]area under the concentration-versus-time curve from the start of dose administration to the last observed quantifiable concentration; [d]time at which the last quantifiable concentration was observed; [e]elimination half-life of mRNA.

DMD Fast Forward. Published on May 19, 2023 as DOI: 10.1124/dmd.122.000980
This article has not been copyedited and formatted. The final version may differ from this version.

Downloaded from dmd.aspetjournals.org at ASPET Journals on April 20, 2024

Table 3. Summary of Tissue Protein Pharmacodynamic Parameters in Sprague Dawley Rats

Matrix	Median TE_{max}[a] (hour)	Mean E_{max}[b] ± SE (μg/g)	Mean $AUEC_{last}$[c] ± SE (hour*μg/g)	Median TE_{last}[d] (hour)	Mean $T_{1/2}$[e] (hour)
Circulatory System					
Heart	24	0.222 ± 0.0371	18.3 ± 2.56	168	NA
Digestive System					
Liver	24	44.2 ± 7.06	1520 ± 157	168	35.3
Jejunum	10	0.185 ± 0.0623	22.2 ± 4.17	168	61.1
Stomach	10	0.0967 ± 0.063	5.47 ± 1.63	168	84.2
Urinary System					
Kidney	72	0.669 ± 0.399	72.1 ± 23.0	168	NA

Downloaded from dmd.aspetjournals.org at ASPET Journals on April 20, 2024

DMD Fast Forward. Published on May 19, 2023 as DOI: 10.1124/dmd.122.000980
This article has not been copyedited and formatted. The final version may differ from this version.

Musculoskeletal System					
Skeletal Muscle	10	0.0642 ± 0.0291	NA	72	NA
Nervous System					
Brain	48	0.0313 ± 0.0198	3.17 ± 1.06	168	NA
Eye	NA	NA	NA	NA	NA
Reproductive System					
Ovary	24	14.7 ± NA	311 ± 8.83	48	NA
Testes	24	0.0727 ± 0.0364	4.20 ± 1.13	72	NA
Uterus	72	0.0892 ± 0.0531	5.72 ± 2.43	168	NA
Immune System					
Lymph Node: Axillary	NA	NA	NA	NA	NA

DMD Fast Forward. Published on May 19, 2023 as DOI: 10.1124/dmd.122.000980
This article has not been copyedited and formatted. The final version may differ from this version.

Downloaded from dmd.aspetjournals.org at ASPET Journals on April 20, 2024

Lymph Node: Inguinal	NA	NA	NA	NA	NA
Lymph Node: Popliteal	NA	NA	NA	NA	NA
Spleen	4	0.327 ± 0.123	8.77 ± 1.05	48	17.1
Thymus	0.83	0.281 ± 0.0764	18 ± 3.70	168	NA
Respiratory System					
Lung	48	0.273 ± 0.0592	33.8 ± 2.51	168	121

NA, Not applicable. Values were not obtained due to insufficient readings and/or unavailability of samples.

[a]Time to reach maximum effect; [b]maximum observed effect; [c]area under the effect-versus-time curve from the start of dose administration to the last observed quantifiable effect; [d]time at which the last quantifiable concentration was observed; [e]elimination half-life of tissue protein.

Downloaded from dmd.aspetjournals.org at ASPET Journals on April 20, 2024

DMD Fast Forward. Published on May 19, 2023 as DOI: 10.1124/dmd.122.000980
This article has not been copyedited and formatted. The final version may differ from this version.

DMD Fast Forward. Published on May 19, 2023 as DOI: 10.1124/dmd.122.000980
This article has not been copyedited and formatted. The final version may differ from this version.

FIGURE LEGENDS

Figure 1. Schematic diagram of LNP with location and chemical structure of Lipid 5. Black arrow indicates the site of radiolabeling with ^{14}C on Lipid 5.

Figure 2. Representative whole-body autoradiographic slices displaying radioactivity measured after intravenous (IV) administration of [^{14}C]Lipid 5-containing LNPs in female Sprague Dawley rats. A single dose of [^{14}C]Lipid 5-containing LNP encapsulating nontranslating factor IX (NT-FIX) mRNA was administered at 2 mg/kg of encapsulated mRNA via 10-min IV infusion. Representative slices shown of slice 4 of whole-body sections at **(a)** 1 hour postdose, **(b)** 10 hours postdose, and **(c)** 168 hours postdose.

Figure 3. Mean detectable radioactivity in blood and tissues in Sprague Dawley rats (1 male and 1 female) as measured by quantitative whole-body autoradiography. (a) circulatory system, **(b)** digestive system, **(c)** urinary system + adrenal gland, **(d)** musculoskeletal system, **(e)** nervous system, **(f)** reproductive system, **(g)** immune system, **(h)** respiratory system. Int, intestinal.

Figure 4. Mean (±SD) detectable plasma and tissue Lipid 5 concentrations after intravenous (IV) administration of Lipid 5-containing LNPs in Sprague Dawley rats as measured by LC-MS/MS. a) circulatory system, **b)** digestive system, **c)** urinary system**, d)** muscoskeletal system, **e)** nervous system, **f)** reproductive system, **g)** immune system, **h)** respiratory system.

Downloaded from dmd.aspetjournals.org at ASPET Journals on April 20, 2024

DMD Fast Forward. Published on May 19, 2023 as DOI: 10.1124/dmd.122.000980
This article has not been copyedited and formatted. The final version may differ from this version.

Figure 5. Mean (±SD) detectable plasma and tissue mRNA concentrations after intravenous (IV) administration of Lipid 5-containing LNPs in Sprague Dawley rats. a) circulatory system, **b)** digestive system, **c)** urinary system**, d)** muscoskeletal system, **e)** nervous system, **f)** reproductive system, **g)** immune system, **h)** respiratory system. BMF, bone marrow femur.

Figure 6. Mean (±SD) detectable tissue intracellular protein concentrations after intravenous (IV) administration of Lipid 5-containing LNPs in Sprague Dawley rats. a) circulatory system, **b)** digestive system, **c)** urinary system, **d)** muscoskeletal system, **e)** nervous system, **f)** reproductive system, **g)** immune system, **h)** respiratory system

Downloaded from dmd.aspetjournals.org at ASPET Journals on April 20, 2024

Figure 1

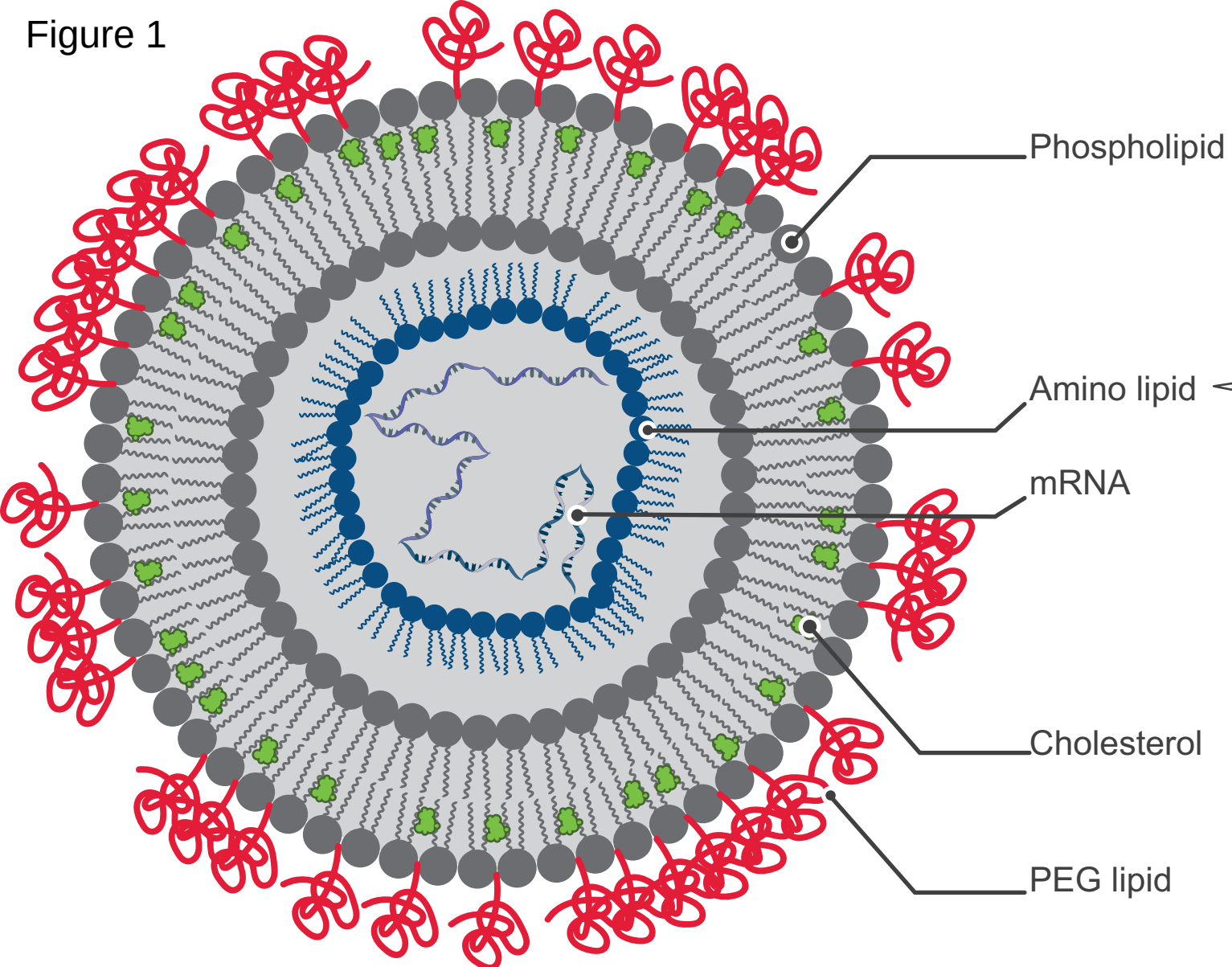

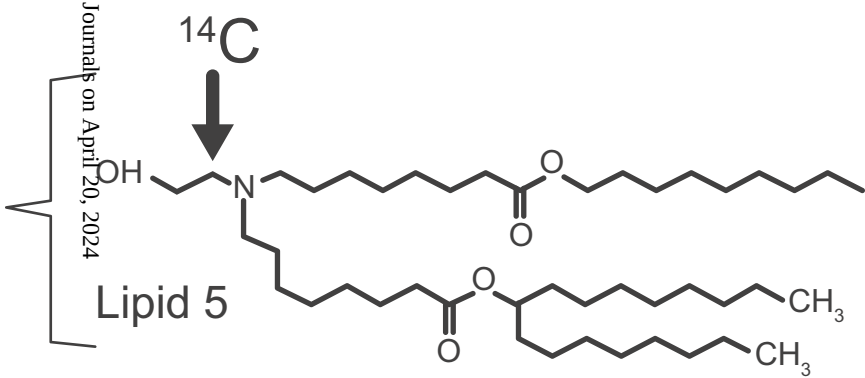

aspetjournals.org at ASPET Journals on April 20, 2024

DMD Fast Forward. Published on May 19, 2023 as DOI: 10.1124/dmd.122.000980
This article has not been copyedited and formatted. The final version may differ from this version.

Figure 2

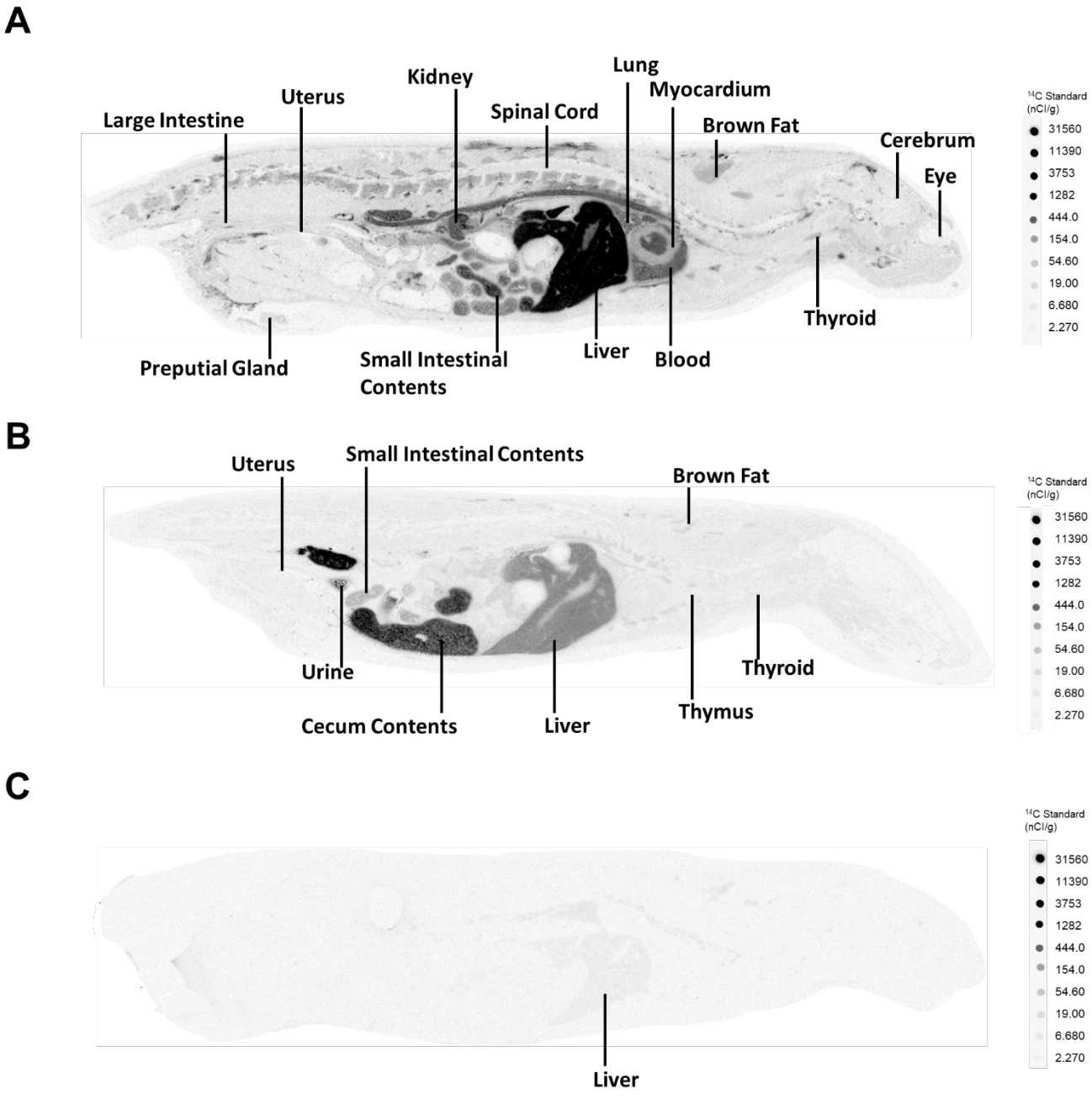

Downloaded from dmd.aspetjournals.org at ASPET Journals on April 20, 2024

Figure 3

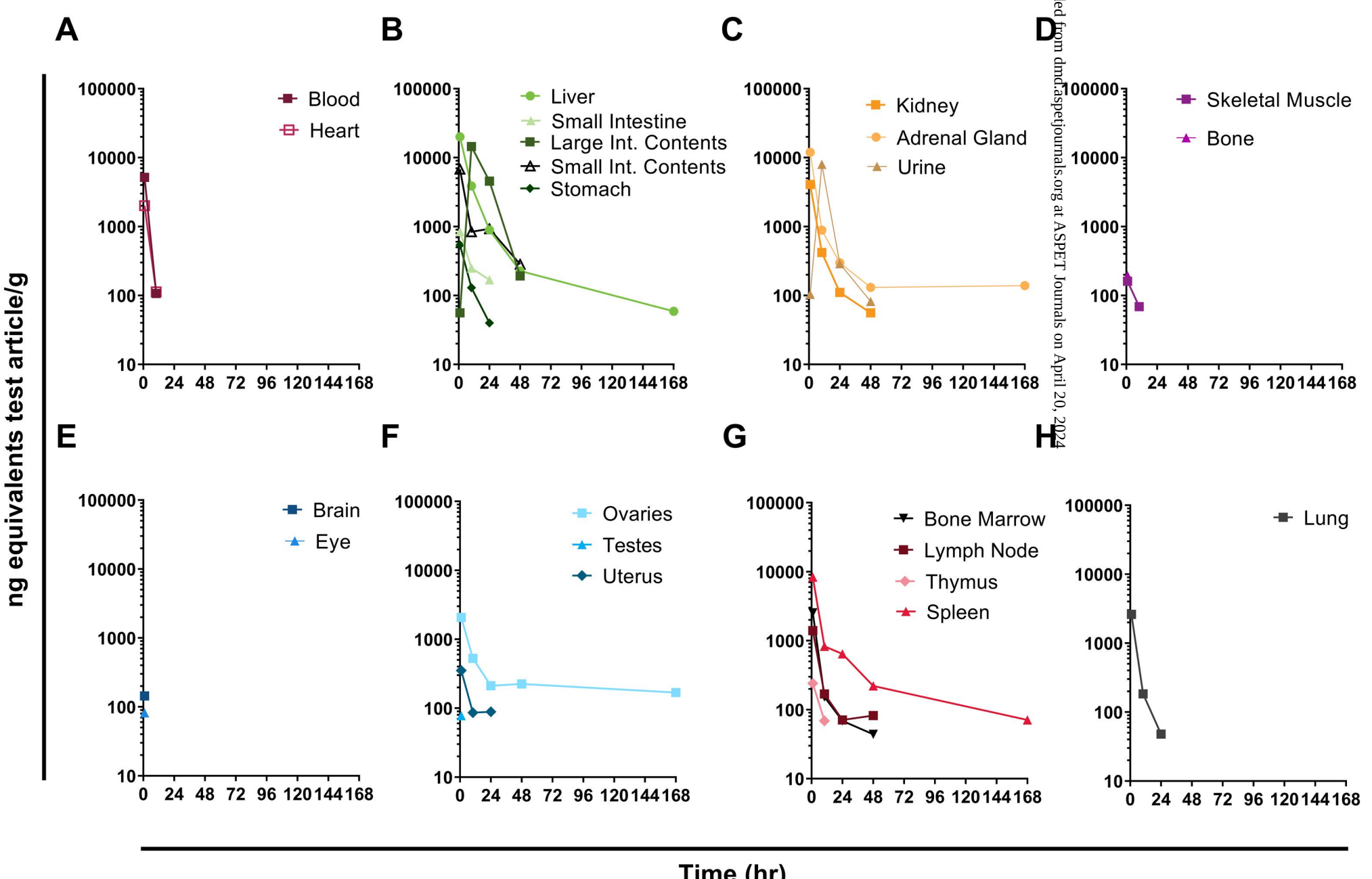

Downloaded from dmd.aspetjournals.org at ASPET Journals on April 20, 2024

Figure 4

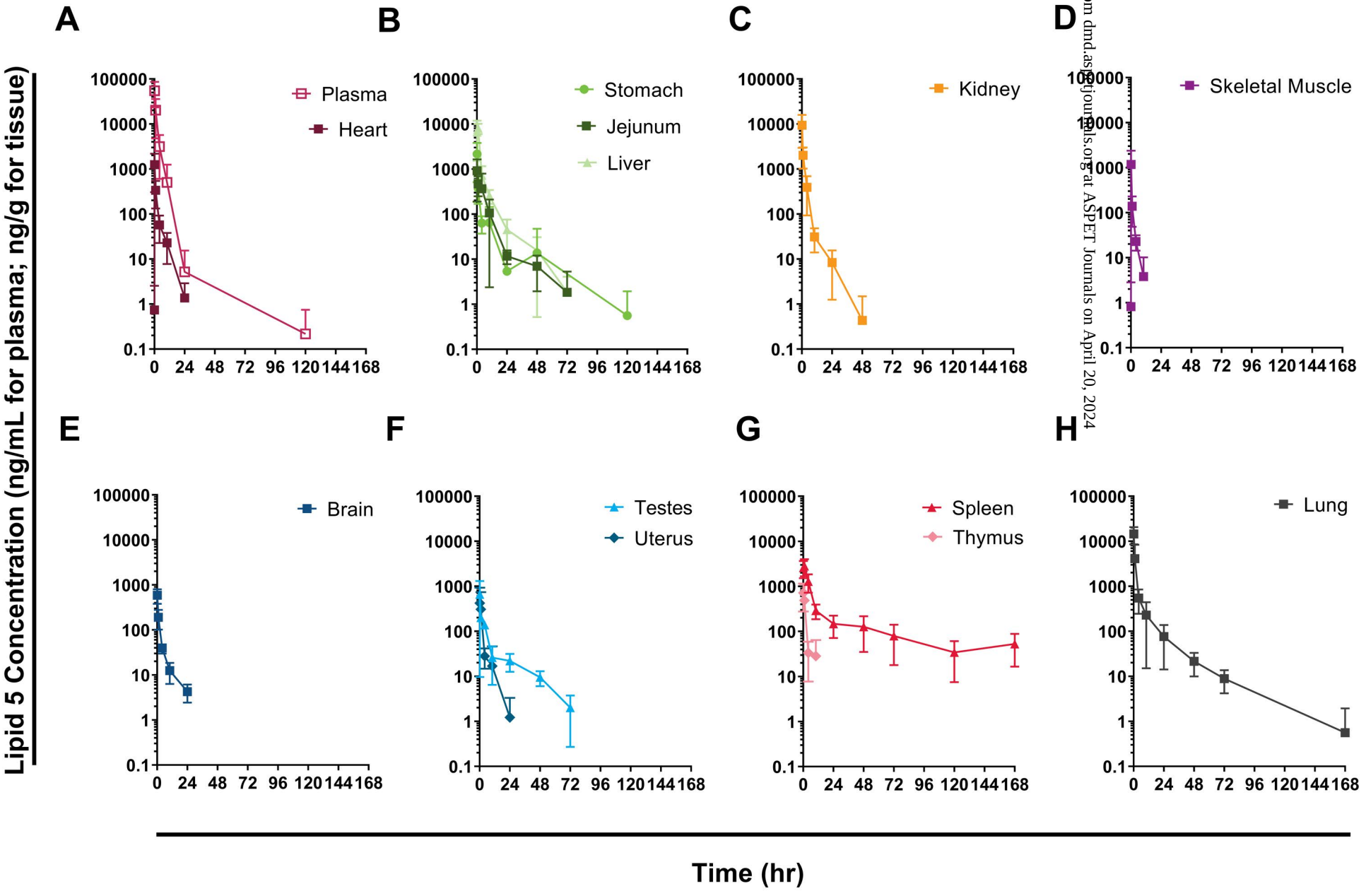

Downloaded from dmd.aspetjournals.org at ASPET Journals on April 20, 2024

Figure 5

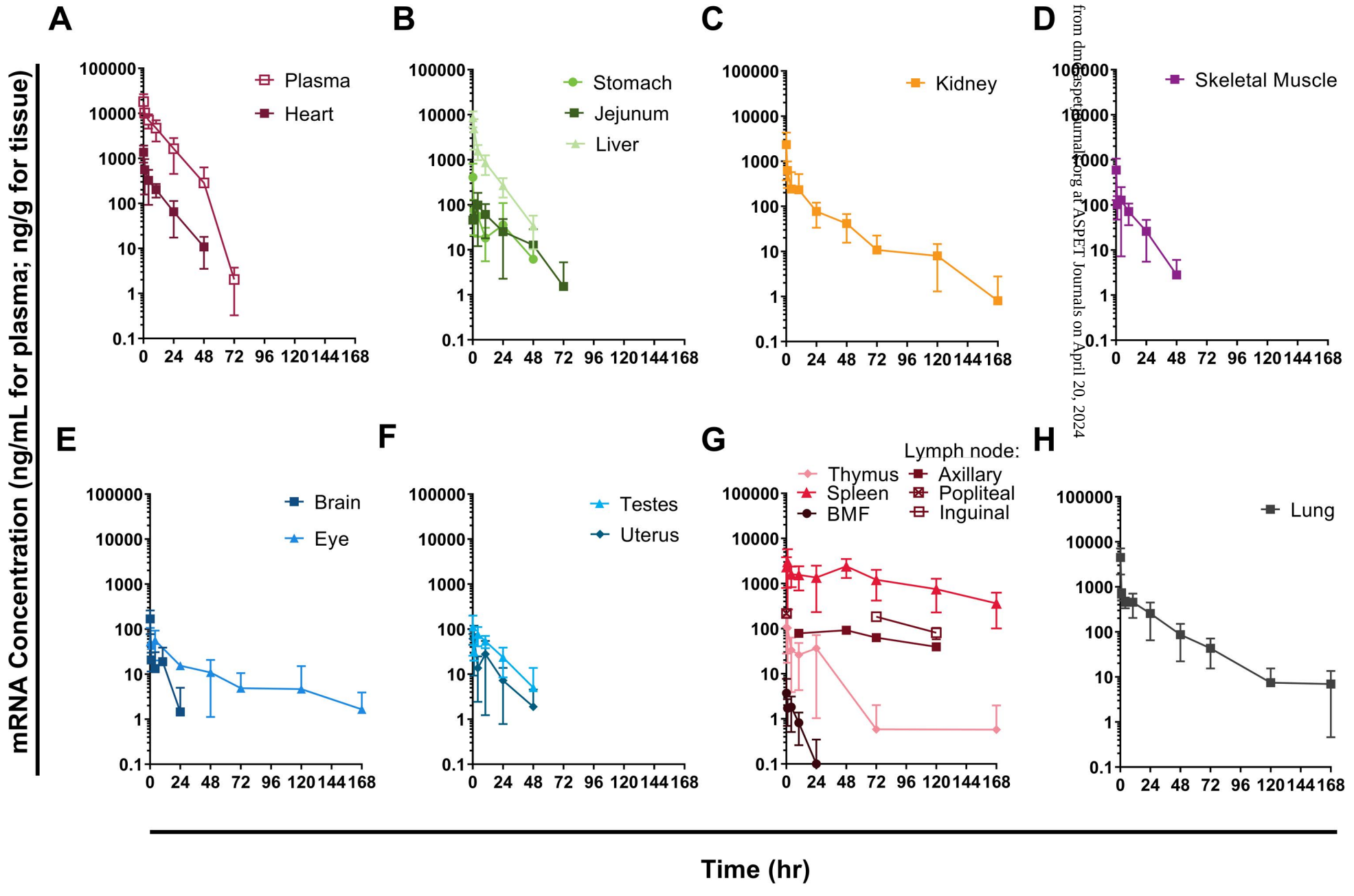

Downloaded from dmd.aspetjournals.org at ASPET Journals on April 20, 2024

Figure 6

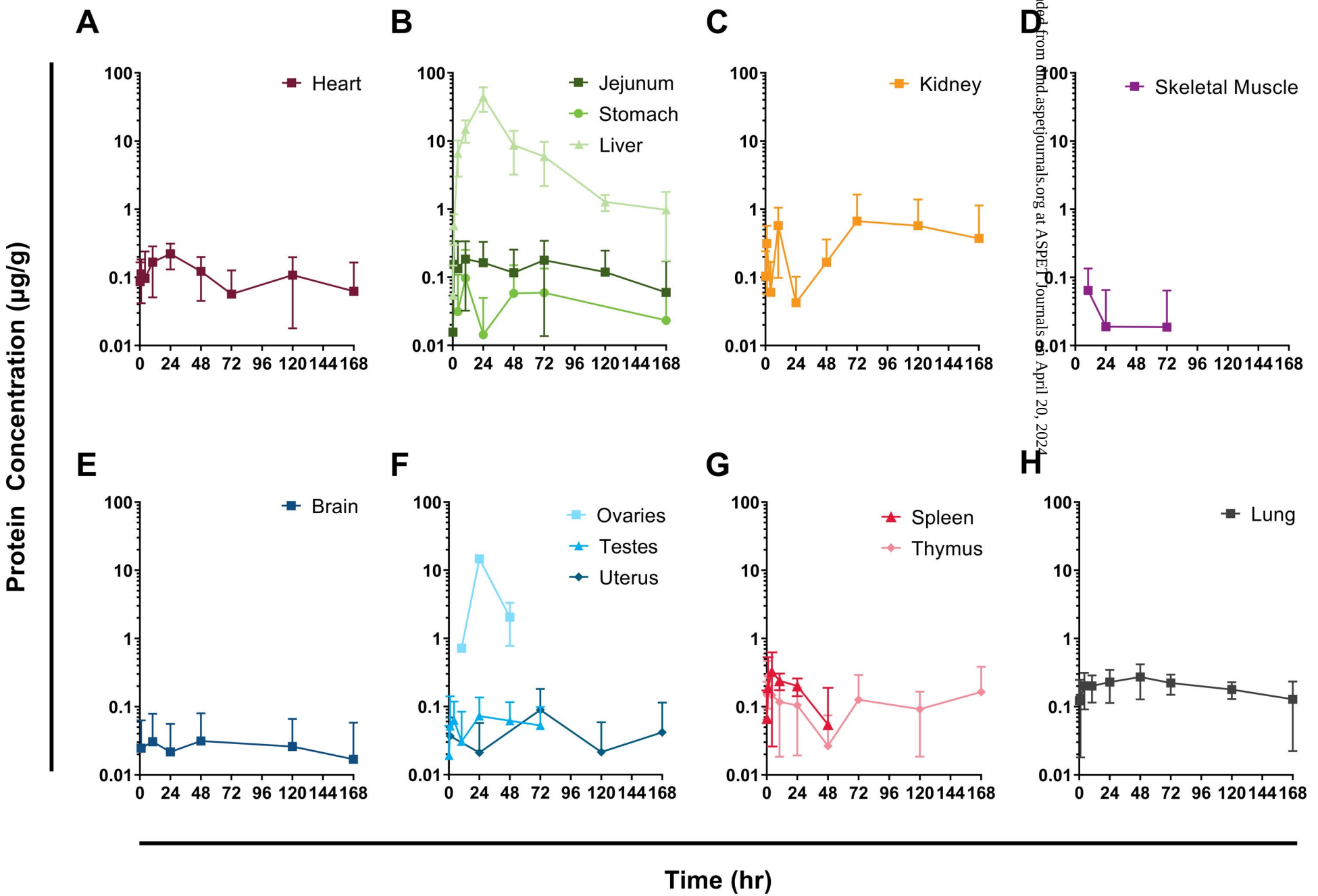

Downloaded from dmd.aspetjournals.org at ASPET Journals on April 20, 2024